*36th EPS Conference on Plasma Phys. Sofia, June 29 - July 3, 2009 ECA Vol.**33E**, P-1.003 (2009)*

Modelling and interpretation of experimental observations of ions accelerated by a high intensity laser pulse illuminating a solid target

Guy Bonnaud[1,2], Tiberio Ceccotti[1], Anna Levy[1], Maria Garbuzova[1,2]

[1]*CEA, IRAMIS, Centre de Saclay, 91191 Gif-sur-Yvette, France*

[2]*CEA, INSTN, same address*

I. Experiments

The chirped pulse amplified UHI Laser provided 650 mJ - 65 fs ultrashort pulses at 0.79 μm central wavelength with a 10 Hz repetition rate. A double plasma mirror [1,2] increases the native peak to pedestal contrast ratio from 10^6 up to 10^{10}, within an overall laser energy transmission of 50% and no measurable distortion of the focal spot. The *p*-polarized laser pulses were focused at 45° incidence angle on Mylar foils with an off-axis f = 300 mm parabola. The intensity on target was at maximum 5.10^{18} W/cm^2 for high contrast (HC) conditions, by using the double plasma mirror optical switch, and twice this value in low contrast (LC) conditions. The single shot ion beam measurements were simultaneously performed for ions emerging normally to the surface of the target from the non illuminated side of the thin foils (FWD) and for ions travelling in the laser counter-propagating direction (BWD), by using two similar Thomson parabola spectrometers. Once dispersed by the magnetic and electric fields of the spectrometer, protons and ions were detected by a two stage 40 mm diameter micro channel plate (MCP, assumed to have a linear response in the ion energy range of interest [3]) coupled to a phosphor screen. The latter was imaged onto a 12 bit CCD camera and ion traces analyzed by using simulated ion parabolas (via the commercial code SIMION).

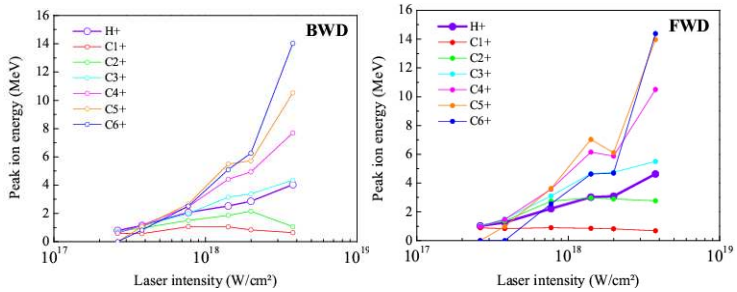

Figure 1 : Peak energy for 0.1 μm thick CH target irradiated with HC pulse

The major result is that C^{5+} and C^{6+} ions have been detected on 10 μm-thick foils only for HC conditions, but not for LC conditions.

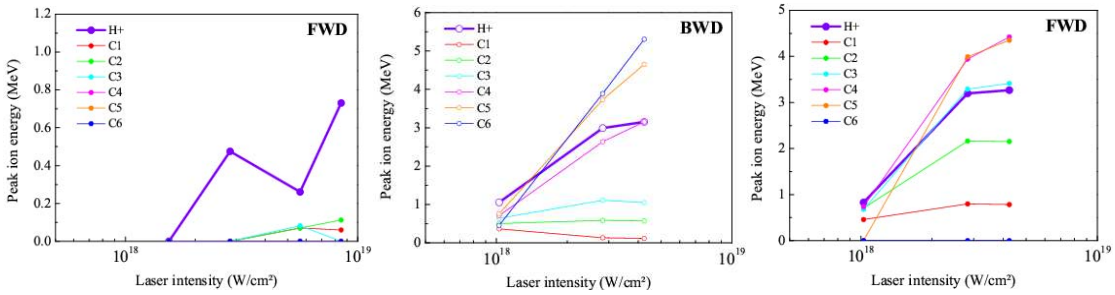

Figure 2: Peak energy for 10 μm thick CH target irradiated with LC (left) and HC (middle and right).

II. Euterpe code and ionisation models

The 1D 3V relativistic particle-in-cell code EUTERPE [4] couples Vlasov to Maxwell equations. Oblique laser incidence is contrived by a code frame where normal incidence is used on a plasma boosted along the laser polarization; going back and forth between the code-lab frames is performed by Lorentz transforming the quantities. This two-decade age code has been upgraded during the last two years, by adding variable weight to macroparticles and a higher order particle-mesh assignment scheme. Compared to standard PIC codes, the numerical noise/self-heating is strongly reduced and the low density areas of the plasma density profiles are better resolved. Binary collisions (not used herein) have been implemented as well with Nanbu method [5] and, more recently, ionizations by tranverse/axial field and electron impact. This paper focuses on this new upgrade.

A Monte-Carlo framework is used by calculating, at each time step Δt, the probability to ionize macroions and by generating uniformly distributed random numbers to decide if ionization occurs via a rejection method. For each ionization event, the macroion charge is increased by +1 and a free macro-electron is created with the ion weight and momentum. The probability is calculated from the local transverse and axial field via the ADK field ionization frequency [6] and from the electron velocities via the Lotz frequency ν_i [7]. Three different macroelectron–macroion collision models have been implemented in each mesh. The *1st model* defines a density and an average kinetic energy for the electron population of one mesh as a whole; excluding electrons with kinetic energies below the ionization potential avoid too slow electrons to ionize to be counted. The *2nd model* is a refinement for variable weight macroparticles of the Ref. [8] model, which from the ionization frequency calculated for the ion densities calculates a maximum number of potentially ionizing macroelectrons. If the ionization probability is low, only a small set of macroelectrons and ions is analyzed, which makes this model based on a predifinite number of likely ionizing electrons the least time consuming. The *3rd model* is based on collisions between pairs of macroelectrons and

macroions. The density and the probability takes into account the unequal colliding particle weights, as for binary collisions [5].

We have verified that for $\nu_i \Delta t < 0.5$ and for a monoenergetic electron beam the three models give identical results as to the ionization dynamics and charge state populations. If a return current is added, ionization is boosted; the 2nd and 3rd models stay identical, whereas the average energy which overestimates the effectively ionizing electrons makes the 1st model amplify ionization. To gauge the relative importance of the accelerated electrons penetrating the target and the electron return current driven by the charge space electric field on ion ionization, we have calculated the ionization frequency $n_e<\sigma v>$ for the high energy accelerated electrons (energy *vs* laser intensity fitted from PIC simulation results reported in Ref. [9]) and the lower energy return current electrons. The sharp increase of the frequencies in Fig. 3 underlines the ionization potentials: 11 to 64 eV for $C \rightarrow C^+ \rightarrow ... \rightarrow C^{4+}$ and 390-490 eV for $C^{4+} \rightarrow C^{5+} \rightarrow C^{6+}$.

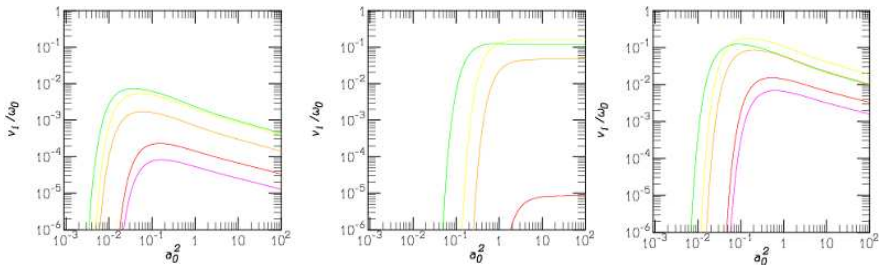

Figure 3: Carbon ionization frequencies (green for $C^+ \rightarrow C^{2+}$, …, purple for $C^{5+} \rightarrow C^{6+}$) in a 100/6 ion density target, as a function of the normalized laser intensity, driven by n_c-density accelerated electrons (left), by the return current driven by n_c-density accelerated electrons (middle) and by target-density accelerated electrons.

III.Simulation results

A $\sin^2$-shaped laser pulse with 120 ω_0^{-1} (= 50 fs) FWHM duration, impinges upon the target at 45 deg. incidence. The electric field has linear P polarization and peaks at $a_0 = 1$ (normalized to $m_e c\omega_0/e$; the associated intensity is $I_0 = 2.2\ 10^{18}$ W/cm^2). The target (65 % C – 35 % H atomic %) is a 6 c/ω_0 (= 0.75 μm) long slab with initial bound electron density equal to 255 n_c (n_c denotes the critical electron density for the incident laser radial frequency ω_0; here $n_c = 1.8\ 10^{21}$ cm^{-3}); C and H densities are 28 and 89 n_c, respectively. An initial top-hat shaped density profile is used for HC whereas LC condition is modelled by a 2 λ_0 1/e-length exponential density profile added on the illuminated side of the target. The field loss due to ionization is modelled by an "ionization" current added to the particle current oriented along the local electric field [10]. The collisional ionization loss is reported to the ionizing macro-electrons by reducing their momentum modulus.

20 % (HC) to 40 % (LC; 6 % absorption induced by ionization) of the incident laser energy is converted into fast electrons. The transverse field penetrates along the skin depth c/ω_{pe} = 0.19 (for C^+H^+ plasma), 0.075 (for $C^{6+}H^+$ plasma) much smaller than the plasma length: transverse field ionization can ionize the target surface only; axial field can ionize up to C^{4+}; collisional ionization appears to be the only process able to ionize carbon to higher charge states C^{5+} and C^{6+}. For LC case, the preplasma is highly charged (C^{6+}) contrasting with the bulk of the target composed with C^{4+} ions exclusively. For HC case, the target is a homogeneous mixing of C^{4+}, C^{5+} and lower density C^{6+} (Fig. 4). The maximum observed energies are 7 MeV for BWD and 3 MeV for FWD but for LC the ion number is 100 times larger than the FWD direction one. This difference induced by a density ramp and a sharp profile is clearly bound to the electron return current. Simulations performed at a_0 = 2 confirm this feature in agreement with the experimental results, making us anticipate that the highly charged ion detection can be a meaurement of the laser contrast quality.

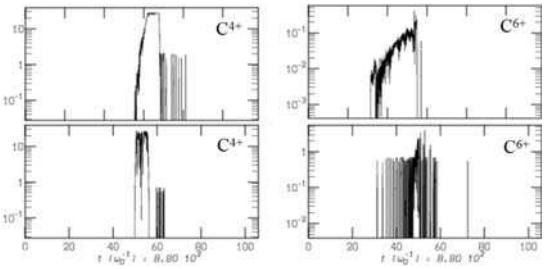

Figure 4: ion density vs $x/(c/\omega_0)$. Initial target location: [50-62] for LC (top), [50-56] for HC (bottom).

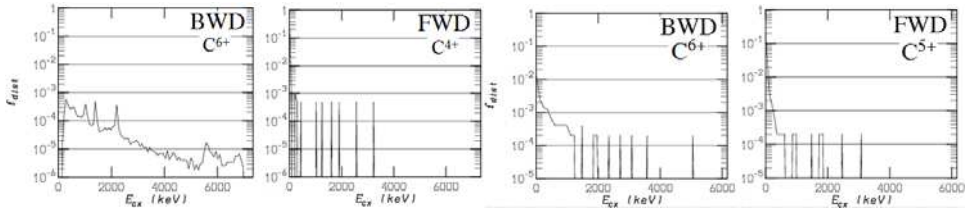

Figure 5: ion energy distribution for charge state indicated on the curves. For LC case (top), HC case (bottom).

IV. References

[1] H. C. Kapteyn et al., Optics Letters 16, 490 (1991).

[2] A. Lévy et al., Optics Letters 32, 310 (2007); T. Ceccotti et al., Phys. Rev. Lett. 99, 585002 (2007).

[3] 3 H. Schwoerer et al., Nature (London) 439, 445 (2006).

[4] Bonnaud G., Reisse C., Nuclear Fusion 26, 633 (1986); Weber S. et al., Phys. Plasmas 8, 387 (2001).

[5] K. Nanbu, Phys. Rev. Lett. 55, 4642 (1997).

[6] M. Ammosov, N.B. Delone, V.P. Krainov, Sov. Phys. JETP 64, 1191 (1986).

[7] H.J. Kunze, Phys. Rev. A 3, 937 (1971).

[8] V. Vahedi et al., Comp.Phys.Comm. 87, 179 (1998); A.J. Kemp et al., Phys. Plasmas 11, 5648 (2004).

[9] E. Lefebvre, G. Bonnaud, Phys. Rev. E 55, 1011(1997).

[10] S.C. Rae, K. Burnett, Phys. Rev. A 46, 1084 (1992).